Lagrangian subgrid-scale modeling applied to evolving firebrand particle transport

By I. D. Santos†, B. Mahato†, B. Bornhoft, S. S. Jain AND N. Yaghoobian†

The transport and deposition of firebrand particles is an important fire spread mechanism in wildland fires. These particles can be transported by wind over large distances and can ignite secondary fires upon landing. The transport of firebrands by wind is a complex, multiscale process that is largely controlled by interactions between the firebrand particles and the atmospheric wind. To account for the complex temporal evolution of atmospheric turbulence over large scales, the use of large-eddy simulation (LES) techniques is necessary. However, filtering of subgrid-scale (SGS) turbulence in LES hinders the accuracy of particle transport models. In this work, we employ a Lagrangian SGS model in an LES framework to investigate the effects of small-scale turbulence on the transport of mass- and size-changing firebrand particles. The impact of SGS turbulence was analyzed by comparing landing and trajectory statistics for firebrand and regular (fixed size and mass) particles under different Stokes numbers. It was found that the presence of SGS turbulence modifies the particle transport behavior, which is characterized by smaller spanwise dispersions but larger travel distances along the streamwise direction compared with particles under no SGS turbulence. As expected, the enhanced velocity field produced by the SGS model has larger influence on the statistics of firebrand particles compared with regular particles due to the time-evolving reduction in particle mass and size induced by pyrolysis.

1. Introduction

Spotting is an erratic fire propagation mechanism associated with the transport of burning or smoldering debris by the wind and its subsequent landing (Tarifa *et al.* 1967). This debris created due to incomplete combustion of the local fuel is lofted into the atmosphere by strong updraft currents near the fire and carried away by the wind far from the main fire front. Once landed, firebrand particles, depending on their combustion condition and temperature, may ignite local fuel and generate secondary fires known as spot fires. The flight distance and landing distribution of firebrands are important parameters to be investigated in order to correctly predict and control the damage of spotting (Hilton *et al.* 2019). The transport of firebrands is a multiscale process controlled by the complex interactions between the firebrand particles and the atmospheric wind. The intermittency and randomness of the spotting process are associated with the turbulent nature of the boundary layer wind and firebrands' variable characteristics as they fly. Firebrands undergo burning processes, which lead to changes in their mass, size, and temperature, affecting the aerodynamic forces on particles along their trajectories. The combination of all these factors makes spotting behavior challenging to predict and control.

Due to the complexity and scale of the atmospheric flow, computational investigation

† Department of Mechanical Engineering, Florida State University

of the spotting process necessitates the use of large-eddy simulations (LES). The review of the literature indicates that in the current LES of firebrand transport, the effect of the subgrid-scale (SGS) turbulence on these inertial particles has been ignored (Bhutia *et al.* 2010; Thurston *et al.* 2017; Anand *et al.* 2018; Hilton *et al.* 2019; Thomas *et al.* 2020). As is evident from fundamental investigations of Lagrangian particle transports (Kuerten & Vreman 2005; Kuerten 2006), ignoring the SGS turbulence affects the accuracy of the particles' trajectory and landing distributions. This is especially important for long-range transport of firebrands in the atmospheric boundary layer (ABL), where the LES grids are inevitably large and, therefore, the amount of filtered-out energy is significant. In addition, since the errors from eliminating the SGS turbulence on traveling particles tend to accumulate over time (Marchioli 2017), ignoring the effect of SGS turbulence is expected to be even more detrimental to the accuracy of long-range spotting simulations. The variation in the size and mass of the firebrand particles during their flight also adds to the complexity of the problem. Hence, the effect of SGS turbulence on the transport of particles cannot be ignored.

Firstly, this work introduces a modeling capability for investigating the effect of the SGS turbulence on flight behavior, transport, and landing distribution of evolving inertial firebrand particles with variable mass and size. The SGS turbulence effect is modeled using an approximate deconvolution-based SGS particle model (Park *et al.* 2017). The model is based on an elliptic differential filter model that calculates SGS velocities based on the resolved LES field. The only model parameter, which refers to the nominal filter width of the differential filter, is obtained dynamically from the resolved velocity field. This model has been selected based on the evidence of improved accuracy of particle statistics in homogeneous-isotropic turbulence compared with DNS for a wide range of Stokes numbers and the simplicity of its implementation. The effect of the mass and size variation of smoldering flying firebrands has been considered through a dynamic burning model (Tse & Fernandez-Pello 1998). Secondly, using this modeling framework, the effect of the SGS turbulence on the trajectory and landing behavior of evolving firebrand particles is investigated for firebrands in an ABL flow over flat terrain and compared against those for regular (fixed mass and size) particles. The modeling details and the simulation setup are explained in Section 2 and 3, respectively. Results and respective discussions are presented in Section 4, followed by concluding remarks in Section 5.

2. Model description

2.1. *The large-eddy simulation model*

For computational modeling of atmospheric turbulence, the parallelized large-eddy simulation model (PALM) (Raasch & Schröter 2001; Maronga *et al.* 2015, 2020) was employed. Using this solver, the turbulent flow is simulated by solving the non-hydrostatic, filtered Navier-Stokes equations under the Boussinesq approximation. The turbulence closure is based on a 1.5-order closure model after Deardorff (1980) for parametrizing the SGS covariance terms. Time-stepping is performed using a third-order Runge-Kutta scheme, while advection terms are discretized using a fifth-order upwind scheme after Wicker & Skamarock (2002). The Monin-Obukhov similarity theory is used for parametrizing the momentum fluxes near the wall. Additional details related to the PALM code and its formulation can be found in Maronga *et al.* (2015, 2020). PALM has widely been used for computational investigations of ABL and urban flows, and various aspects of the code have been extensively validated and documented elsewhere [Letzel *et al.* (2008); Park

et al. (2012); Letzel *et al.* (2012); Park *et al.* (2013); Yaghoobian *et al.* (2014); Lo & Ngan (2015); Duan & Ngan (2019); Duan *et al.* (2019)].

2.2. *Modeling of the effect of SGS turbulence on Lagrangian inertial particles*

The effect of the SGS turbulence on Lagrangian inertial particles is modeled based on a dynamic SGS model (Park *et al.* 2017). The model introduces the SGS velocity components, u_i', in terms of the LES resolved velocity $\bar{u}_i$ as

$$u_i' = u_i - \bar{u}_i = \frac{\partial}{\partial x_j}\left(b^2 \frac{\partial \bar{u}_i}{\partial x_j}\right). \tag{2.1}$$

Here, the model parameter b, which represents the filter size of the elliptical filter, is calculated using a kinetic-energy-marching dynamic procedure. This procedure is formulated by constraining the SGS kinetic energy from the differential filter (DF) model to be equal to that calculated from the LES model (i.e., $k_{\mathrm{SGS}}^{\mathrm{DF}} = k_{\mathrm{SGS}}^{\mathrm{LES}}$). This leads to the expression

$$\mathcal{T}_{kk}^{\mathrm{LES}} - b^2 \frac{\partial^2 \mathcal{T}_{kk}^{\mathrm{LES}}}{\partial x_\ell \partial x_\ell} - 2b \frac{\partial b}{\partial x_m} \frac{\partial \mathcal{T}_{kk}^{\mathrm{LES}}}{\partial x_m} = R_{kk}, \tag{2.2}$$

where R_{kk} is an auxiliary tensor of the form

$$R_{ij} = 2b^2 \, \frac{\partial \bar{u}_i}{\partial x_k} \frac{\partial \bar{u}_j}{\partial x_k} + \frac{\partial}{\partial x_n}\left(b^2 \frac{\partial \bar{u}_i}{\partial x_n}\right) \frac{\partial}{\partial x_p}\left(b^2 \frac{\partial \bar{u}_j}{\partial x_p}\right). \tag{2.3}$$

In Eq. (2.2), $\mathcal{T}_{ij}^{\mathrm{LES}} = \overline{u_i u_j} - \bar{u}_i \bar{u}_j$ is the SGS stress tensor obtained from the resolved velocity field. Following Park *et al.* (2017), the parameter b is considered to be spatially uniform, which guarantees the modeled SGS velocity field to be incompressible. This also allows the calculation of b from a simpler, volume-averaged version of Eq. (2.2) as

$$\langle \alpha \rangle b^4 + \langle \beta \rangle b^2 - \langle \gamma \rangle = 0. \tag{2.4}$$

The coefficients in Eq. (2.4) are given by

$$\alpha = \frac{\partial^2 \bar{u}_k}{\partial x_\ell \partial x_\ell} \frac{\partial^2 \bar{u}_k}{\partial x_m \partial x_m}, \qquad \beta = 2 \frac{\partial \bar{u}_k}{\partial x_\ell} \frac{\partial \bar{u}_k}{\partial x_\ell} + \frac{\partial^2 \mathcal{T}_{kk}^{\mathrm{LES}}}{\partial x_\ell \partial x_\ell}, \qquad \gamma = \mathcal{T}_{kk}^{\mathrm{LES}}, \tag{2.5}$$

with $b^2 > 0$ corresponding to the physically relevant root. The influence of SGS turbulence on the trajectory of a particle is strongly dependent on the particle's mass and size (Marchioli 2017; Mollicone *et al.* 2019), considered through the particle's Stokes number. The Stokes number of the particles is calculated based on the LES filter size Δ, i.e., $Stk_\Delta = \tau_{\mathrm{p}}/\tau_\Delta$ (Marchioli 2017), where $\tau_{\mathrm{p}} = \rho_{\mathrm{p}} d_{\mathrm{p}}^2/18\mu$ and $\tau_\Delta \sim \left(\Delta^2/\varepsilon\right)^{1/3}$, ρ_{p} and d_{p} are the density and diameter of the particle, μ is the dynamic viscosity of the fluid, and ε is the resolved energy dissipation. Due to the pyrolysis process, firebrand particles undergo changes in mass and size along their trajectories, inducing reductions in their Stokes numbers over time. Changes in the firebrands' mass and size are tracked in time using a dynamical burning model based on the d-squared law (Tse & Fernandez-Pello 1998), explained in the following section.

2.3. *Firebrand tracking and burning model*

Firebrand particles are tracked individually across the flow, and their positions and velocities are obtained by solving the conservation of linear momentum in a Lagrangian frame of reference according to $m_{\mathrm{p}}(\mathrm{d}\mathbf{V}_{\mathrm{p}})/\mathrm{d}t = \mathbf{F}_{\mathrm{D}} + \mathbf{F}_{\mathrm{g}}$. In this equation, m_{p} and $\mathbf{V}_{\mathrm{p}}(=$

$\mathrm{d}\mathbf{r}_\mathrm{p}/\mathrm{d}t$) are the firebrand mass and velocity vector, respectively, with $\mathbf{r}_\mathrm{p}$ being the position vector of the particle. $\mathbf{F}_\mathrm{g}$ and $\mathbf{F}_\mathrm{D}$ are the gravitational and drag forces, respectively, defined as

$$\mathbf{F}_\mathrm{D} = \frac{1}{2} C_\mathrm{D}\ \rho_\mathrm{air}\ A_\mathrm{p}\ |\mathbf{V}_\mathrm{r}|^2\ \frac{\mathbf{V}_\mathrm{r}}{|\mathbf{V}_\mathrm{r}|}, \tag{2.6}$$

$$\mathbf{F}_\mathrm{g} = (\rho_\mathrm{p} - \rho_\mathrm{air}) \forall_\mathrm{p}\ \mathbf{g}, \tag{2.7}$$

where $\mathbf{V}_\mathrm{r} (= \mathbf{V}_\mathrm{w} - \mathbf{V}_\mathrm{p})$ represents the three-dimensional (3D) relative velocity vector between the firebrand velocity ($\mathbf{V}_\mathrm{p}$) and the velocity of the wind at the particle location ($\mathbf{V}_\mathrm{w}$) that is obtained from the LES. C_D is the drag coefficient, $A_\mathrm{p} (= \pi d_\mathrm{p}^2/4)$ is the particle's projected area, $\mathbf{g}$ is the gravitational acceleration, $\forall_\mathrm{p}$ is the volume of the particle, and ρ_air is the density of air. All air properties are calculated as functions of the instantaneous firebrand temperature. This allows for considering temperature-driven variations in buoyancy due to pyrolysis via Eq. (2.7). It is assumed that additional forces induced by the presence of pyrolysis are small compared with the external drag forces. These forces could be caused by updrafts and gas ejections originating from the firebrands surface. However, since it is considered that the pyrolysis occurs under smoldering combustion, the chemical reactions leading to such events are much slower and less intense than other combustion processes, such as flaming or glowing combustion (Finney *et al.* 2021). In addition, the firebrands analyzed in this work are relatively small and have short pyrolysis lifetimes compared with their total flight times. The instantaneous velocity of the flow at the particle location ($\mathbf{V}_\mathrm{w}$) is obtained from the enhanced ($\bar{u}_i + u_i'$) LES flow field by linear interpolations of the 3D velocities in time and space using the time separation between the flow snapshots and the spatial resolution of the LES data. Tracking of the firebrands was performed in a postprocessing step, using the velocity field obtained from the LES. The input flow field consists of snapshots of the instantaneous flow velocity components, separated by an interval of 0.5 sec. The cumulative volume of the flying firebrand particles to the volume of the fluid domain (volume loading) is small ($\sim 10^{-10}$), and therefore a one-way coupling between the LES and the particle models (where only flow affects the particles) is considered sufficient (Elghobashi 1994; Kuerten 2016).

Since, in this work, particles are assumed to be perfectly spherical and non-rotational, there will be no Magnus effect (Mehta 1985) acting on the firebrands. Therefore, no lift force is considered in the particle trajectory model. In addition, the released firebrands are large enough so that additional force components (i.e., Basset force and Saffman lift) are assumed to be negligible compared with drag and gravitational forces (Wang & Squires 1996). The drag coefficient (C_D) in Eq. (2.6) is based on an empirical relation for a smooth sphere (Clift & Gauvin 1971), as adopted for the spherical firebrand trajectory modeling in Anthenien *et al.* (2006),

$$C_\mathrm{D} = \frac{24}{Re_d}\left(1 + 0.15\ Re_d^{0.687}\right) + \frac{0.42}{\left(1 + 4.25 \times 10^4 Re_d^{-1.16}\right)}, \qquad Re_d < 3 \times 10^5, \tag{2.8}$$

where Re_d refers to the Reynolds number based on the firebrand diameter. In order to account for changes in firebrands' mass and size due to pyrolysis effects, a uniform radial regression model is employed (Tse & Fernandez-Pello 1998; Anthenien *et al.* 2006). A schematic of the burning model is presented in Figure 1.

The model is steered by a single parameter that controls both the size and mass

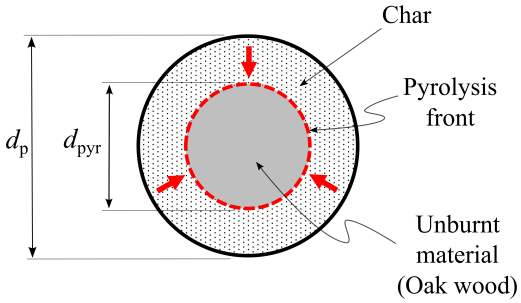

FIGURE 1. Schematic of the burning model for spherical firebrands. d_{p} and d_{pyr} represent the external and the pyrolysis front diameters, respectively.

regression rates of each firebrand. This parameter β, called the regression coefficient, is based on an experimentally correlated equation presented by Williams (1985),

$$\beta = \beta_0 \left(1 + 0.276\ Re_d^{0.5} Pr^{1/3}\right), \tag{2.9}$$

where β_0 is the burning coefficient for oak wood under no wind and Pr is the Prandtl number of the surrounding air. Following Tse & Fernandez-Pello (1998), the density of char is assumed to be small and therefore negligible compared to that of the unburned material. Therefore, the mass of the particle m_{p} is computed based on the volume of the firebrand delimited by the pyrolysis front. The diameter of the pyrolysis front, d_{pyr}, and the external diameter of the particle that includes the charred portion, d_{p}, are then found from

$$\frac{\mathrm{d}\left(d_{\mathrm{pyr}}^2\right)}{\mathrm{d}t} = -\beta, \tag{2.10}$$

$$\frac{\mathrm{d}\left(d_{\mathrm{p}}^4\right)}{\mathrm{d}t} = -\chi\beta^2 t, \tag{2.11}$$

where t is the flight time and $\chi = 2\sqrt{3}$ is a fitting coefficient. Firebrands are assumed to be made of rigid oak wood for which the thermodynamic properties are obtained from Tse & Fernandez-Pello (1998). Following Tse & Fernandez-Pello (1998), firebrands burn until their mass reaches 24% of their initial mass at the release point (Tarifa *et al.* 1967), after which the pyrolysis process ceases, and the particles lose their heat to the environment. At this stage, the mass of the firebrands is kept constant until the end of their trajectory.

3. Simulation set-up

The atmospheric flow simulations were performed on a rectangular domain with periodic boundary conditions in the horizontal directions and no-slip and Neumann boundary conditions, respectively, at the bottom and top. Grid and domain sensitivity analyses were conducted and a 600 m(x) $\times$ 300 m(y) $\times$ 600 m(z) domain with a horizontal grid size of $\Delta_x = \Delta_y = 3$ m was selected. In the vertical direction, the grid size $\Delta_z = 3$ m was kept constant up to a height of 60 m, above which a stretching factor of 1.08 was applied. Firebrand particles with initial Stokes numbers of 0.3 and 0.5 and regular (fixed mass and size) particles of the same Stokes numbers were injected randomly over time and

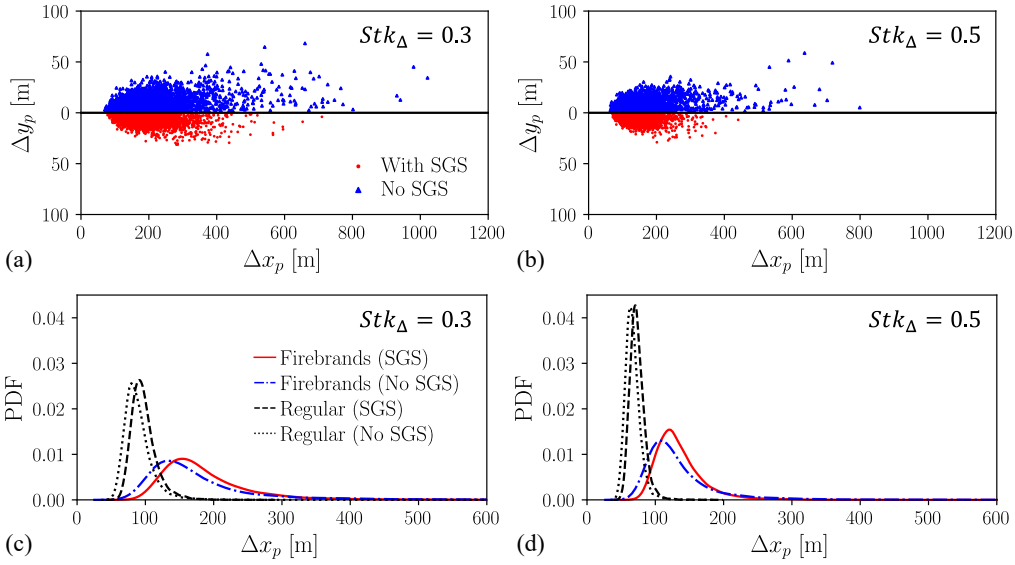

FIGURE 2. Discrete distribution of the distance traveled by firebrand particles with and without the SGS turbulence effects with (a) $Stk_\Delta = 0.3$ and (b) $Stk_\Delta = 0.5$. Δx_p and Δy_p, respectively, show the distance traveled by the particles in the stream and spanwise directions. Probability density functions (PDF) of streamwise travel distance for firebrand and regular particles with (c) $Stk_\Delta = 0.3$ and (d) $Stk_\Delta = 0.5$.

horizontal space, with an initial velocity equal to the average freestream wind velocity in the domain (i.e., 10 m/s). Considering that the flow is periodic in the stream and spanwise directions, the particles were released over the whole extent of the horizontal domain at a fixed height $z = 20$ m. The random release of particles in time happened over 280 s, which corresponds to about five eddy turnover times in the domain. Through a sensitivity analysis, it was found that a total of $36,000$ particles for each case can provide statistical convergence, for example, in terms of the mean and standard deviation of the particle landing positions.

4. Results and discussions

To investigate how the SGS turbulence affects the LES transport of the firebrand particles in the ABL, we first investigate the differences in the landing and travel distance statistics of the particles released in the same flow, with and without the SGS turbulence. Figure 2(a,b) shows the discrete distribution of the distance traveled by the firebrand particles of $Stk_\Delta = 0.3$ and 0.5. Complementing these results, Figure 2(c,d) presents the probability density function (PDF) of the streamwise travel distance of these particles. For both Stokes numbers, the PDF plots indicate that firebrand particles traveling through the enhanced (resolved + SGS) velocity field are more likely to travel a larger distance in the streamwise direction. However, Figure 2(a,b) indicates that these particles disperse less compared to the particles without the SGS effects. Comparison of the PDF plots of the particles' spanwise travel distance (not shown) and Figure 2(a,b) indicate that particles in the enhanced flow travel and disperse less in the crossflow direction. By introducing spatial intermittencies to the turbulence field, the SGS model is able to regenerate smaller turbulent structures, which may lead to smaller regions

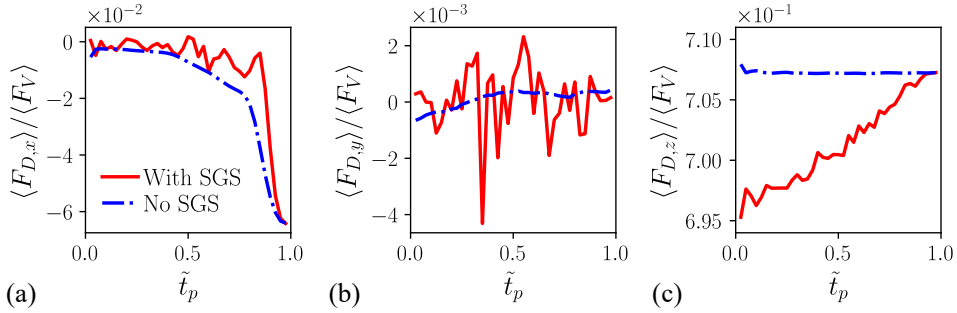

FIGURE 3. Comparison of the ratios of the instantaneous ensemble-averaged drag force components to the ensemble-averaged resultant vertical force along (a) x, (b) y, and (c) z directions for firebrand particles of $Stk_\Delta = 0.3$.

of preferential particle concentration (Park *et al.* 2017). The accumulation of particles along these smaller structures may be the reason why a smaller particle dispersion was observed under the presence of SGS velocity for the analyzed range of Stokes number. Additional insight into this behavior could be drawn from a more in-depth analysis of the coherent structures within the turbulent flow. Future investigations on this topic will be conducted by evaluating the impact of the SGS model on the integral time scales of both the flow and the particles. The reduction in particle spreading under the effect of SGS turbulence is also observed for regular particles [black lines in Figure 2(c,d)]. However, since the mass and size of these particles are fixed (unlike firebrand particles that become lighter due to the pyrolysis process throughout their flight), they are less susceptible to the effects of the surrounding flow and travel significantly shorter distances regardless of the Stokes number. In general, as expected, larger particles land sooner and closer to each other and the effect of the SGS turbulence on their landing statistics decreases because they are more resilient to the acceleration induced by the small-scale turbulence [Figure 2(c,d)].

To investigate the differences in the particle travel distance and landing statistics, it is desired to study the drag force experienced by the particles as they travel through the resolved and enhanced LES flow fields. Figure 3 compares the components of the instantaneous ensemble-averaged drag force acting on the firebrand particles of $Stk_\Delta = 0.3$ throughout their flight with and without the effects of the SGS turbulence. Since the ratio of horizontal to vertical force acting on each particle is a defining factor of its trajectory, results in Figure 3 are presented as ratios of each ensemble-averaged drag component with respect to the ensemble-averaged resultant vertical forces acting on the particles. The resultant vertical force is $\langle F_\mathrm{V} \rangle = \left\langle \sqrt{F_{\mathrm{D},z}^2 + F_\mathrm{g}^2} \right\rangle$, where $F_{\mathrm{D},z}$ and F_g are the vertical drag and the weight acting on the particle, respectively. The ensemble average (represented by the angle brackets) was performed over all particles at fixed intervals of normalized flight time $\tilde{t}_p$ of each particle. From Figure 3, it is observed that the additional SGS velocities in the enhanced field lead to instantaneous fluctuations in all components of the drag force, leading to the deviation of the particles' trajectory in the two flows. Since the ratios along all directions are below unity, this indicates that the resultant vertical force is larger than the individual drag components. Therefore, the combined effects of the vertical drag and the weight play a major role in defining the trajectories and eventual deposition behavior of the firebrands, which explains the strong dependency of the deposition behavior on the Stokes number (Figure 2). It can be seen

that particles in the enhanced flow, in general, experience smaller magnitudes of mean streamwise drag forces during their flight, which correspond to smaller decelerations along the streamwise direction as they settle toward the ground. This explains the longer travel distance of these particles. However, Figure 3(c) indicates that particles in the enhanced flow also experience smaller mean vertical drag. Since a positive vertical drag indicates resistive forces against the settling of the particles, the smaller values of drag experienced by the particles in the enhanced flow indicate that these particles would tend to settle faster towards the ground. This effect would partially counter the effect of the reduced magnitude of streamwise drag, which may relate to the smaller maximum travel distances observed for the enhanced flow (Figure 2). The observed drag force fluctuations should be investigated in more detail considering the integral time scale of the turbulent flow in the path of the falling particles at different heights in comparison to the integral time scale of the turbulent transport of the ensemble particles. The large fluctuations of the instantaneous drag forces also lead to an increase in the probability of occurrence of larger values of particle acceleration for the enhanced flow compared with those obtained from the resolved flow. This is indicated by the analysis of particle acceleration PDFs, which show wider PDFs for all components of particle acceleration (not shown).

5. Conclusions

In this work, the impact of the addition of a structural SGS model on the behavior of firebrand and regular particles was evaluated for two Stokes numbers. Firebrand particles were characterized by having time-evolving mass and size according to regression coefficients based on experimental correlations. Landing and trajectory statistics for particles released in grid-filtered (LES) and enhanced (LES+SGS) velocity fields were analyzed, and the main differences observed between the two cases were addressed.

Regarding the effect of the SGS model, particles transported with the enhanced flow had larger travel distances along the streamwise direction but smaller travel distances along the spanwise direction compared with those travelling in the filtered flow. The larger travel distances were attributed to a decrease in the average drag force magnitude in the streamwise direction. For the range of Stokes numbers analyzed, the presence of SGS turbulence led to a decrease in the dispersion of landing positions in the streamwise and spanwise directions. This effect is considered to be attributed to the effect of the smaller turbulence structures introduced by the model, which could lead to smaller regions of preferential particle concentration within the flow.

When compared with regular particles, firebrand particles had significantly larger travel distances and spreading along both streamwise and spanwise directions. This behavior is led by the reduction in particle mass and size due to the pyrolysis process, which makes the firebrands more susceptible to the effects of SGS turbulence. Deeper studies are required to fully understand the effects of the SGS turbulence on the firebrand transports. In addition, the evaluation of the performance between the structural and stochastic SGS models under firebrand-related conditions and the analysis of non-spherical firebrand shapes can help researchers better understand the underlying physics. It is also desired to investigate the impact of the SGS turbulence on the temperature and pyrolysis rate of the firebrands and the potential of spotting ignition induced by the deposited still-alive particles. These topics will be explored in the future.

Acknowledgments

The authors acknowledge use of computational resources from the Yellowstone cluster awarded by the National Science Foundation to CTR and the HPC resources at the Florida State University.

REFERENCES

Anand, C., Shotorban, B. & Mahalingam, S. 2018 Dispersion and deposition of firebrands in a turbulent boundary layer. *Int. J. Multiphas. Flow* **109**, 98113.

Anthenien, R. A., Stephen, D. T. & Fernandez-Pello, A. C. 2006 On the trajectories of embers initially elevated or lofted by small scale ground fire plumes in high winds. *Fire Safety J.* **41**, 349–363.

Bhutia, S., Ann Jenkins, M. & Sun, R. 2010 Comparison of firebrand propagation prediction by a plume model and a coupled–fire/atmosphere large–eddy simulator. *J. Adv. Model Earth Sy.* **2**.

Clift, R. & Gauvin, W. 1971 Motion of entrained particles in gas streams. *Can. J. Chem. Eng.* **49**, 439–448.

Deardorff, J. W. 1980 Stratocumulus-capped mixed layers derived from a three-dimensional model. *Bound.-Lay. Meteorol.* **18**, 495–527.

Duan, G., Jackson, J. & Ngan, K. 2019 Scalar mixing in an urban canyon. *Environ. Fluid Mech.* **19**, 911–939.

Duan, G. & Ngan, K. 2019 Sensitivity of turbulent flow around a 3-D building array to urban boundary-layer stability. *J. Wind Eng. Ind. Aerod.* **193**, 103958.

Elghobashi, S. 1994 On predicting particle-laden turbulent flows. *Appl. Sci. Res.* **52**, 309–329.

Finney, M. A., McAllister, S. S., Grumstrup, T. P. & Forthofer, J. M. 2021 Wildland fire behaviour: dynamics, principles and processes. CSIRO Publishing.

Hilton, J., Sharples, J., Garg, N., Rudman, M., Swedosh, W. & Commins, D. 2019 Wind-terrain effects on firebrand dynamics. In *23rd Int. Congr. Model. Simul.* Canberra, Australia.

Kuerten, J. 2006 Subgrid modeling in particle-laden channel flow. *Phys. Fluids* **18**, 025108.

Kuerten, J. 2016 Point-particle DNS and LES of particle-laden turbulent flow a state-of-the-art review. *Flow Turbul. Combust.* **97**, 689-713.

Kuerten, J. & Vreman, A. 2005 Can turbophoresis be predicted by large-eddy simulation? *Phys. Fluids* **17**, 011701.

Letzel, M. O., Helmke, C., Ng, E., An, X., Lai, A. & Raasch, S. 2012 LES case study on pedestrian level ventilation in two neighbourhoods in Hong Kong. *Meteorol. Z.* **21**, 575–589.

Letzel, M. O., Krane, M. & Raasch, S. 2008 High resolution urban large-eddy simulation studies from street canyon to neighbourhood scale. *Atmos. Environ.* **42**, 8770–8784.

Lo, K. & Ngan, K. 2015 Characterising the pollutant ventilation characteristics of street canyons using the tracer age and age spectrum. *Atmos. Environ.* **122**, 611–621.

Marchioli, C. 2017 Large-eddy simulation of turbulent dispersed flows: a review of modelling approaches. *Acta Mech.* **228**, 741-771.

Maronga, B., Banzhaf, S., Burmeister, C., Esch, T., Forkel, R., Fröhlich, D., Fuka, V., Gehrke, K. F., Geletič, J., Giersch, S. *et al.* 2020 Overview of the PALM model system 6.0. *Geosci. Model Dev.* **13**, 1335–1372.

Maronga, B., Gryschka, M., Heinze, R., Hoffmann, F., Kanani-Sühring, F., Keck, M., Ketelsen, K., Letzel, M. O., Sühring, M. & Raasch, S. 2015 The parallelized large-eddy simulation model (PALM) version 4.0 for atmospheric and oceanic flows: model formulation, recent developments, and future perspectives. *Geosci. Model Dev.* **8**, 2515–2551.

Mehta, R. D. 1985 Aerodynamics of sports balls. *Annu. Rev. Fluid Mech.* **17**, 151–189.

Mollicone, J., Sharifi, M., Battista, F., Gualtieri, P. & Casciola, C. 2019 Particles in turbulent separated flow over a bump: effect of the Stokes number and lift force. *Phys. Fluids* **31**, 103305.

Park, G., Bassenne, M., Urzay, J. & Moin, P. 2017 A simple dynamic subgrid-scale model for LES of particle-laden turbulence. *Phys. Rev. Fluids* **2**, 044301.

Park, S.-B., Baik, J.-J., Raasch, S. & Letzel, M. O. 2012 A large-eddy simulation study of thermal effects on turbulent flow and dispersion in and above a street canyon. *J. Appl. Meteorol. Clim.* **51**, 829–841.

Park, S.-B., Baik, J.-J. & Ryu, Y.-H. 2013 A large-eddy simulation study of bottom-heating effects on scalar dispersion in and above a cubical building array. *J. Appl. Meteorol. Clim.* **52**, 1738–1752.

Raasch, S. & Schröter, M. 2001 PALM-A large-eddy simulation model performing on massively parallel computers. *Meteorol. Z.* **10**, 363–372.

Tarifa, C. S., Pérez del Notario Martínez de Marañón, P., García Moreno, F. & Rodríguez Villa, A. 1967 Transport and combustion of firebrands. Final report of grants FG-SP-114 and FG-SP-146 Vol. II.

Thomas, C., Sharples, J. & Evans, J. 2019 The terminal-velocity assumption in simulations of long-range ember transport. *Math. Comput. Simulat.* **175**, 96–107.

Thurston, W., Kepert, J. D., Tory, K. J. & Fawcett, R. J. 2017 The contribution of turbulent plume dynamics to long-range spotting. *Int. J. Wildland Fire* **26**, 317–330.

Tse, S. & Fernandez-Pello, A. 1998 On the flight paths of metal particles and embers generated by power lines in high winds - a potential source of wildland fires. *Fire Safety J.* **30**, 333-356.

Wang, Q. & Squires, K. D. 1996 Large eddy simulation of particle deposition in a vertical turbulent channel flow. *Int. J. Multiphas. Flow* **22**, 667–683.

Wicker, L. J. & Skamarock, W. C. 2002 Time-splitting methods for elastic models using forward time schemes. *Mon. Weather Rev.* **130**, 2088–2097.

Williams, F. A. 1985 *Combustion Theory*. CRC Press.

Yaghoobian, N., Kleissl, J. & Paw U, K. T. 2014 An improved three-dimensional simulation of the diurnally varying street-canyon flow. *Bound.-Lay. Meteorol.* **153**, 251–276.